Supplementary information for Universal evolution of a viscous-capillary spreading drop

Sumesh P. Thampi,[1] Ignacio Pagonabarraga,[2] Ronojoy Adhikari,[3] and Rama Govindarajan[4]

[1] *Department of Chemical Engineering, Indian Institute of Technology Madras, Chennai 600036, India.*
[2] *Department de Fisica Fonamental, Universitat de Barcelona, Avinguda Diagonal 647, E-08028 Barcelona, Spain*
[3] *The Institute of Mathematical Sciences, CIT Campus, Chennai 600113, India*
[4] *TIFR Centre for Interdisciplinary Sciences, Tata Institute of Fundamental Research, Hyderabad 500075, India*[*]

Diffuse Interface Model and Hydrodynamics

The drop spreading process is simulated using a standard approach to describe the dynamics of binary fluid systems. An order parameter ψ is defined as the normalised difference in density to distinguish the two fluids. The model is a coupled system of equations comprising Cahn-Hilliard equation (CHE) describing the evolution of the order parameter and the Navier-Stokes equation (NSE) describing the hydrodynamics for an incompressible fluid [1–4],

$$\partial_t \psi + \nabla\cdot(\mathbf{u}\psi) = \nabla\cdot(M\nabla\mu) \tag{1}$$

$$\partial_t(\rho\mathbf{u}) + \nabla\cdot(\rho\mathbf{u}\mathbf{u}) = -\nabla p + \eta\nabla^2\mathbf{u} + \psi\nabla\mu \tag{2}$$

together with the continuity equation for the density. In the above, p stands for the pressure, η is the shear viscosity. Here the mobility M relates the order parameter flux and the chemical potential gradient driving the diffusion. While the order parameter is advected by the flow field in Eq. 1, the gradients in the order parameter give rise to forces driven by chemical potential, and extra stresses appear in the NSE, Eq. 2 [5].

The equilibrium thermodynamics of the fluid is described by the Landau free-energy functional [1, 6]

$$F(\psi) = \int \left(\frac{A}{2}\psi^2 + \frac{B}{4}\psi^4 + \frac{K}{2}\left|\nabla\psi\right|^2\right) d\mathbf{r}, \tag{3}$$

with $A < 0$, $B > 0$ and $\mathbf{r}$ stands for the spatial dimensions. Two uniform solutions $\psi = \pm\sqrt{A/B}$ coexists across a fluid interface for this free energy functional form. The interfacial thickness

$$\xi = \sqrt{2K/A} \tag{4}$$

and the interfacial energy

$$\gamma = \frac{2}{3}\sqrt{2KA^3/B^2} \tag{5}$$

are controlled by three parameters A, B, and K [2]. Here $\mu = A\psi + B\psi^3 - K\nabla^2\psi$ is the chemical potential.

We use a hybrid algorithm by combining the lattice Boltzmann (LB) method for hydrodynamics and method of lines for the order parameter dynamics [7]. Force densities such as the divergences of order parameter stresses are included in the modified LB method used here [8]. We use a $D3Q15$ model and collision integral is a single relaxation time (τ) approximation. The viscosity is obtained as $\eta = \tau c_s^2$ where $c_s = 1/\sqrt{3}$ is the sound speed in LB units. The spatial discretization of the CHE is based on a finite-volume formulation [9] and this set of equations is temporally integrated using a Runge-Kutta algorithm. The interested reader is referred to [7] for a detailed description of this method.

The wall is placed at the $\frac{1}{2}$ location, as is usual in the bounce back schemes used to represent wall in LB method [10]. Desired contact angles are obtained as discussed in [11, 12]. In short, the solid-fluid surface tension is introduced by defining free energy functional of the form $\frac{C}{2}\psi_s^2 + H\psi_s$ where ψ_s is the value of order parameter at the wall. Minimization of the energy functional near the wall gives $C\psi_s + H = K\nabla\psi\cdot\mathbf{n}$ where $\mathbf{n}$ is normal to the wall. By tuning the parameters C and H we can modify the properties of the surface. It is found sufficient to retain only the linear term of the surface energy functional [11, 12]. We use a second order central difference formula to calculate the normal derivative of order parameter at the wall.

We have used the following definition and method to determine the interface and contact line. We define the interface between the two fluids to be where the order parameter, $\psi = 0$ and extract the shape of the drop at every time step as the contour line of $\psi = 0$. Consistent with our quasi-steady assumption of the evolution of the drop, we fit an equation of a circle on this contour and calculate the contact radius and contact angle. However, we have verified that our results are independent of the (i) definition of interface and (ii) the procedure adopted to calculate the instantaneous contact radius and contact angle. At long times, the drop reaches equilibrium and one may then obtain static contact angle. It is possible to analytically calculate the static contact angle as a function of H from the theory proposed above using a free energy minimisation as described in [11, 12]:

$$\cos\theta = \frac{1}{2}\left[(1+h)^{3/2} - (1-h)^{3/2}\right]. \tag{6}$$

where H is redefined as $h = H\sqrt{2/KB}$. We have compared our computational results with this expression for a satisfactory match.

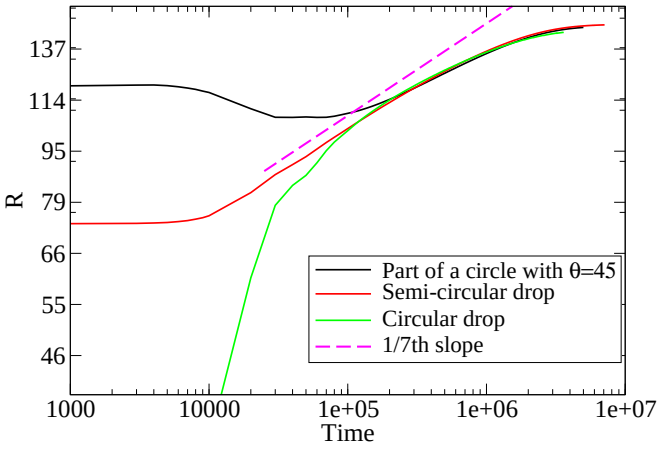

FIG. 1. Asymptotic behaviour is same for drop spreading with three different initial conditions: (i) drop shape as part of a circle with $\theta = 45°$, (ii) a semicircular drop with $\theta = 90°$ and (iii) a full circle with $\theta = 180°$. Algebraic growth followed by exponential relaxation may be observed in all cases. In these simulations $\theta_e = 30, \eta = 0.15, \eta_r = 1, M = 0.1, \sigma = 9.4 \times 10^{-4}$

The late stage dynamics of the drop is unaffected by the choice of initial shape of the drop. We show this explicitly in Fig. 1. Tests were done with three different initial conditions (i) drop shape as part of a circle with initial contact angle $\theta = 45°$, (ii) a semicircular drop with initial contact angle $\theta = 90°$ and (iii) a circular drop with initial contact angle $\theta = 180°$. Case (i) has the largest, case (ii) has intermediate and case (iii) has negligible initial contact area. Results of these simulations are shown in Fig. 1. It may be seen that after the initial transients the drop spreads analogously in all the cases implying that the initial conditions are not important in studying the long term spreading behaviour.

More results from numerical simulations

We have varied the relevant parameters of interest over a wide range. Here. Figs. 2-5 show the spreading kinetics for a wide range of dimensionless parameters. Specifically, Reynolds number varies from $O(10^{-5})$ to $O(10)$, Capillary number varies from $O(10^{-5})$ to $O(0.1)$ and Ohnesorge number varies from $O(10^{-3})$ to $O(10)$. It may be helpful to note that in various drop spreading experiments in the reported literature, Oh varies from $O(10^{-3})$ to $O(0.1)$, which we have covered in our simulations. As observed in the plots, for the case of $\theta_e = 20°$ we find TVH and then a transition to the exponential regime in all the cases except when inertia becomes important. Large Re numbers and small Oh number indicate the regime where inertia becomes relevant in spreading kinetics. We then see systematic deviations from TVH and even non-monotonic spreading as shown in Fig. 5. In the case of $\theta_e = 60°$, TVH completely disappears, and we find spreading faster than that predicted by TVH and then an exponential regime as shown in Fig. 2(b) and Fig. 3(b). This is same as the behaviour that we illustrate via Eq. 4 and Fig. 3 in our manuscript. Again, when inertial effects become important, as shown in the first case in Fig. 3(b), we observe deviations and non monotonic spreading behaviour consistent with observations in [13]. Also, high Reynolds number may not be a relevant regime experimentally for drops typically smaller than capillary length.

* rama@tifrh.res.in

[1] P. M. Chaikin and T. C. Lubensky, *Principles of Condensed Matter Physics* (Cambridge, 1995).
[2] V. M. Kendon, M. E. Cates, I. Pagonabarraga, J. C. Desplat, and P. Bladon, J. Fluid. Mech. **440**, 147 (2001).
[3] G. K. Batchelor, *An Introduction to Fluid Dynamics* (Cambridge University Press, 1967).
[4] L. D. Landau and E. M. Lifshitz, *Fluid Mechanics* (Pergamon Press, 1959).
[5] D. Anderson, G. McFadden, and A. Wheeler, Annu. Rev. Fluid Mech. **30**, 139 (1998).
[6] J. S. Rowlinson and B. Widom, *Molecular Theory of Capillarity* (Dover Publications, 1982).
[7] S. P. Thampi, I. Pagonabarraga, and R. Adhikari, Phys. Rev. E **84**, 046709 (2011).
[8] R. W. Nash, R. Adhikari, and M. E. Cates, Phys. Rev. E **77**, 026709 (2008).
[9] B. Rotenberg, I. Pagonabarraga, and D. Frenkel, Europhys. Lett. **83**, 34004 (2008).
[10] S. Succi, *The Lattice Boltzmann Equation for Fluid Dynamics and Beyond* (Oxford University Press, 2001).
[11] J. C. Desplat, I. Pagonabarraga, and P. Bladon, Comput. Phys. Commun. **134**, 2001 (2001).
[12] A. J. Briant, P. Papatzacos, and J. M. Yeomans, Phil. Trans. R. Soc. Lond. A **360**, 485 (2002).
[13] H. Ding and P. D. M. Spelt, J. Fluid Mech. **576**, 287 (2007).

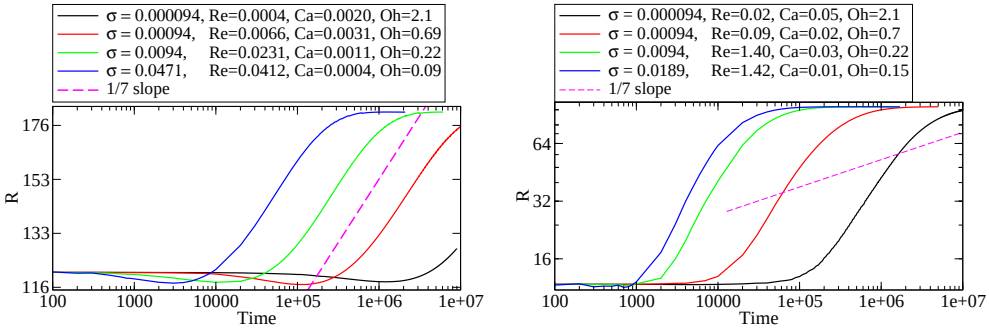

(a) $\theta_e = 20°$ (b) $\theta_e = 60°$

FIG. 2. As surface tension increases,the driving force increases and the spreading is faster. Other parameters used are $\eta = 0.15$ and $M = 0.1$. (a) For $\theta_e = 20°$. TVH is followed by exponential relaxation. The smallest surface tension, $\sigma = 0.000094$, demands large computational time to reach final stages of spreading. The second case $\sigma = 0.00094$ is used in Fig. 1(c) in the main paper. (b) For $\theta_e = 60°$, which does not show TVH law, is also shown for comparison.

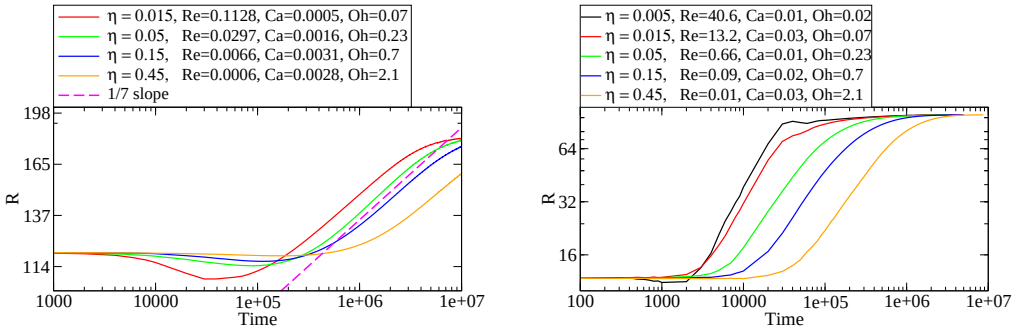

(a) $\theta_e = 20°$ (b) $\theta_e = 60°$

FIG. 3. As viscosity increases, spreading is slower, as expected. Other parameters used are $M = 0.1, \sigma = 9.4 \times 10^{-4}$. (a) For $\theta_e = 20°$. TVH law, and the transition to exponential regime can be observed. The first case, $\eta = 0.015$ is shown in Fig 1(a) of the manuscript. (b) For $\theta_e = 60°$ is also shown for comparison.

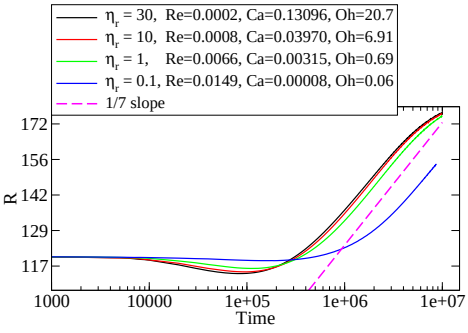

FIG. 4. Here viscosity of the drop and the surrounding fluid is changed independently. η_r is defined as the ratio of the viscosity of the drop to that of the external fluid. As η_r increases, spreading becomes faster. Parameters used in these simulations are $\theta_e = 20°$, $\eta = 0.15$ (surrounding fluid), $M = 0.1, \sigma = 9.4 \times 10^{-4}$. TVH law, and then the transition to non-algebraic relaxation can be observed.

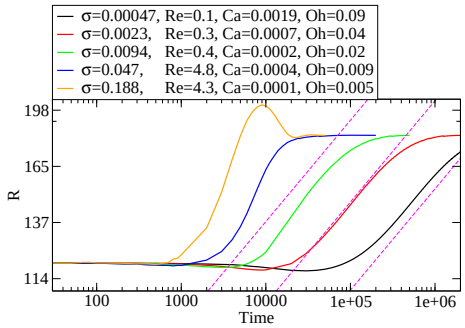

FIG. 5. Effect of inertia on the rate of spreading. When surface tension increases, after a point inertial effects become important giving rise to deviations from Tanner's law, and even nonmonotonic rate of spreading. Parameters used are $\theta_e = 20°$, $M = 1, \eta = 0.015$.

Effect of various parameters on the spreading process: Ohnesorge number, $Oh = \sqrt{Ca/Re} = \eta/\sqrt{(h\sigma\rho)}$ is defined in each case where $Ca = \eta U/\sigma$ is the capillary number and $Re = \rho U h/\sigma$ is the Reynolds number. The spreading speed at the beginning of the algebraic growth is used as the characteristic velocity U, which continuously decreases as spreading proceeds. h is the initial height of the drop, η is the viscosity, σ is the surface tension and ρ is the density of the fluid.